Influence of Nanosize Hole Defects and their Geometric Arrangements on the Superfluid Density in Atomically Thin Single Crystals of Indium Superconductor

Mengke Liu,[1] Hyoungdo Nam,[1] Jungdae Kim,[1,2] Gregory A. Fiete,[3,4] and Chih-Kang Shih[1]
[1]Department of Physics, The University of Texas at Austin, Austin, Texas 78712, USA
[2]Department of Physics and EHSRC, University of Ulsan, Ulsan 680-749, South Korea
[3]Department of Physics, Northeastern University, Boston, Massachusetts 02115, USA
[4]Department of Physics, Massachusetts Institute of Technology, Cambridge, Massachusetts 02139, USA

(Received 11 January 2021; revised 11 May 2021; accepted 4 August 2021; published 17 September 2021)

Using Indium $\sqrt{7} \times \sqrt{3}$ on Si(111) as an atomically thin superconductor platform, and by systematically controlling the density of nanohole defects (nanometer size voids), we reveal the impacts of defect density and defect geometric arrangements on superconductivity at macroscopic and microscopic length scales. When nanohole defects are uniformly dispersed in the atomic layer, the superfluid density monotonically decreases as a function of defect density (from 0.7% to 5% of the surface area) with minor change in the transition temperature T_C, measured both microscopically and macroscopically. With a slight increase in the defect density from 5% to 6%, these point defects are organized into defect chains that enclose individual two-dimensional patches. This new geometric arrangement of defects dramatically impacts the superconductivity, leading to the total disappearance of macroscopic superfluid density and the collapse of the microscopic superconducting gap. This study sheds new light on the understanding of how local defects and their geometric arrangements impact superconductivity in the two-dimensional limit.

DOI: 10.1103/PhysRevLett.127.127003

Superconducting ground states are known to be robust against nonmagnetic disorder [1], in the weakly disordered 3D bulk case. However, in a highly disordered regime, both the transition temperature T_C and the superfluid density (SFD) can be significantly suppressed by disorder induced vortex pinning and scattering centers [2–6]. A conventional superconductor (SC) in the two-dimensional (2D) limit has a low T_C and low SFD, resulting in fragile superconductivity [7–9]. Previous investigations using highly disordered amorphous and granular films have also shown a rapid suppression of both T_C and the SFD with thickness reduction, eventually resulting in a superconductor-insulator transition [3,10–17]. The emergence of single crystal films, however, reveals surprises: at a thickness of only few monolayers, Pb films still show remarkably high superfluid rigidity with robust superconductivity [18–21], indicating the need for a close examination of how superfluid rigidity disappears with increasing of disorder in single crystal superconducting films in the 2D limit. Intuitively, in the single atomic layer limit, one anticipates that local defects would have a profound impact on superconductivity [1]. But exactly "how" such defects manifest at different length scales in 2D superconductivity remains unexplored territory. With the rapid discovery of different atomically thin single crystal superconductors [20,22,23], addressing how the defect formation at a microscopic level influences the superconductivity in the 2D limit becomes ever critical and timely.

Using indium $\sqrt{7} \times \sqrt{3}$ on Si(111) as an atomically thin superconductor platform [Fig. 1(a)] [24–28], we control the formation of one specific type of defects, nanometer-size hole defects, in terms of density and their geometric arrangements, and investigate the superconductivity from microscopic to macroscopic length scales. Microscopically, we probe the local superconducting gap using scanning tunneling microscopy/spectroscopy (STM/STS) [Fig. 1(b)] and macroscopically, we probe the SFD using a double coil mutual inductance measurement [Fig. 1(c)] [2,29–31]. Most significantly, we found that these nanohole defects have a profound impact on the superconductivity at different length scales. When these nanohole defects are uniformly dispersed in the 2D film, we found that the SFD decreases

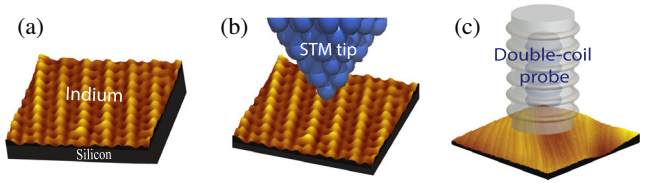

FIG. 1. Schematic illustration of methodology. (a) Indium adatoms on Si(111) and reconstruction into the $\sqrt{7} \times \sqrt{3}$ phase. (b) Microscopic probe of scanning tunneling microscope. Both the probe apex and the tunneling region are in nm scale. (c) Macroscopic probe of the double-coil mutual inductance system. Both the probe coil size and the sample size are in mm scale.

monotonically as increasing of defect density while T_c, measured both microscopically and macroscopically, remains relatively robust. However, at higher defect concentrations, when these point defects are organized into defect chains that separate the 2D surface into regions of enclosed 2D patches, both the SFD and quasiparticle gap vanish, down to the lowest temperature of our measurements (~2.3 K).

The double-coil measures the temperature dependent complex sheet conductivity $\Upsilon(T) = [\sigma_1(T) + i\sigma_2(T)]d$, where d is the sample thickness, in our case determined using STM (see Supplemental Material [32]), and $\sigma_1 + i\sigma_2$ is the usual complex conductivity [2,18,29–31,33,34]. The real part σ_1 reflects the dissipative process caused by vortex motion, and the imaginary part σ_2 is related to the SFD n_s, through $\sigma_2 = n_s e^2/m\omega$ [8]. It is customary to refer to $1/\lambda^2 = \mu_0 n_s e^2/m$ as the SFD (as they are proportional), and we adopt this convention. This setup also allows us to directly measure the superfluid phase rigidity J_s, through $J_s = \hbar^2 d/4e^2\mu_0 k_B \lambda^2$. A detailed description of the double-coil setup and SFD calculation can be found in the Supplemental Material [32]. As both the STM/STS and double coil probes are *in situ* and noncontact, the sample crystallinity is maintained and undesirable effects from electrical contact fabrication are avoided in *in situ* transport measurements [24,25,28,35]. By applying these two techniques on the same sample, a direct comparison between microscopic and macroscopic SC behavior can be made.

Starting from a pristine single crystal indium $\sqrt{7} \times \sqrt{3}$ layer on Si(111), we introduce defects as an independent control parameter (see Supplemental Material [32]). Figures 2(a) to 2(d) show the topography of sample No. 1 to sample No. 4 with increasing defects density. The inset atomic images show that all four samples are in the $\sqrt{7} \times \sqrt{3}$ phase. The percentage of the hole defects refers to the surface area fraction occupied by the voids. In addition, the area fraction of extra islands is also labeled. Figures 2(e) and 2(f) show typical zoomed-in images of hole and island defects, both of which are in nanometer scales and cause imperfection on a continuous film. Figure 2(g) shows the temperature dependent superfluid density $1/\lambda(T)^2$, for sample No. 1 to sample No. 4 and Fig. 2(h) shows the corresponding real part σ_1 evolution. Using the two-fluid model fitting, $1/\lambda^2(T) = 1/\lambda^2(0\ \mathrm{K})[1 - (T/T_c)^4]$, on sample No. 1 [Fig. 2(g)], the zero-temperature SFD can be estimated: $1/\lambda^2(0\,\mathrm{K}) = 3.4\,\mu\mathrm{m}^{-2}$. From the temperature dependent SFD one can calculate the phase rigidity, $J_s(\mathrm{T})$. Following Emery and Kivelson [9], we evaluate the ratio between the characteristic phase-ordering temperature [$0.9 \times J_s(0\ \mathrm{K})$ for a 2D system] and the superconductivity transition temperature, as it parametrizes the strength and importance of phase fluctuations in the superconductivity transition. The ratio is roughly 2 for sample No. 1, indicating a regime where the phase fluctuations play an important role, even for a nearly perfect crystalline film. Note this ratio is markedly different from

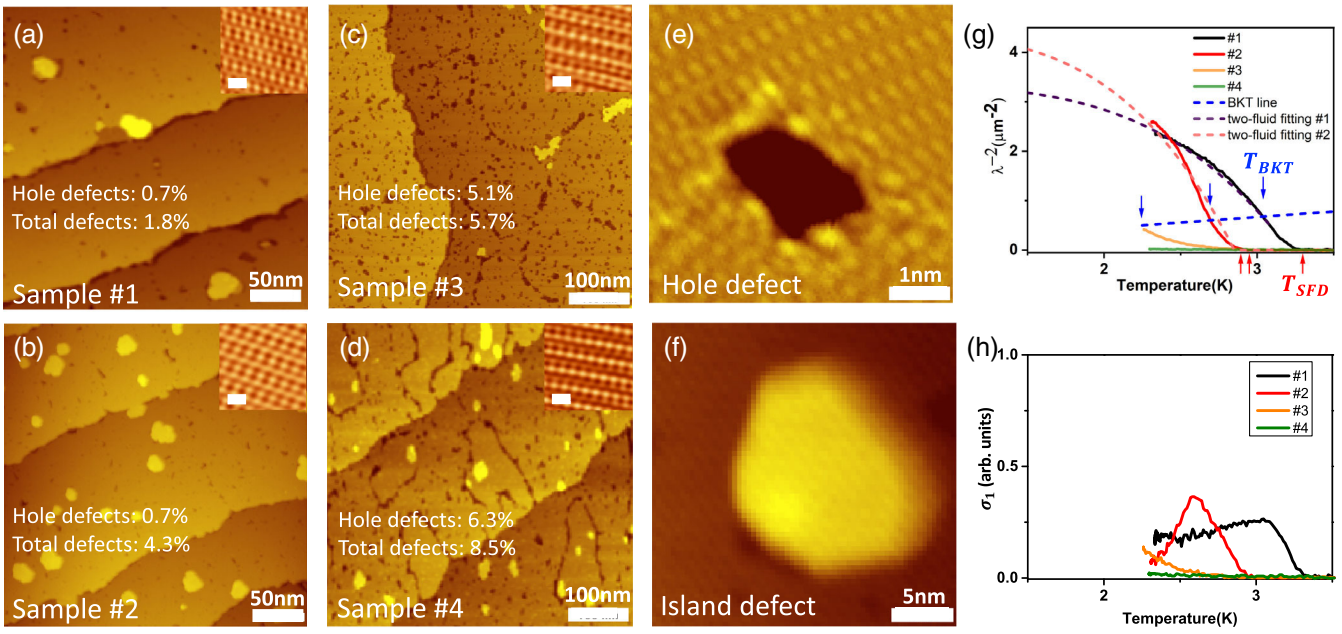

FIG. 2. Temperature dependent superfluid density. (a)–(d) Topography of indium $\sqrt{7} \times \sqrt{3}$ samples with varying defect densities. The top right insets show their corresponding atomic images where the scale bar is 1 nm. (e)–(f) Topographic image of hole and island defects. (g) Temperature dependent superfluid density for sample No. 1 to No. 4. The two-fluid model fitting is used for sample No. 1 and No. 2 to extrapolate the SFD at 0 K. The blue dashed line is the universal BKT line. (h) The temperature dependent σ_1 for sample No. 1 to No. 4.

an earlier study of few-monolayer Pb films whose superfluid rigidity is more than an order of magnitude higher [18], and for bulk Pb, this ratio is more than 2 orders of magnitude [9].

The temperature dependent SFD in the extreme 2D limit can be described by the Berezinskii–Kosterlitz–Thouless (BKT) theory adapted to the SC scenario [36–39], which is that the universal BKT line with a slope of $8\pi\mu_0 k_B/d\Phi_0^2$ intersects $1/\lambda(T)^2$ at the BKT transition temperature, i.e., $T_{\mathrm{BKT}} = (\pi/2)J_s$. At this temperature thermally excited vortices start to proliferate and destroy the quasi-long-range order. A standard BKT theory would predict a sudden jump in the SFD from zero to a finite value at T_{BKT} [36,38,39]. However, such a sudden jump in the SFD is absent here; instead, the change is gradual, varying across a finite temperature range, suggesting that the behavior here does not follow the traditional BKT theory [40]. Because of this smooth transition, a finite SFD can still be detected above T_{BKT}. We define the critical temperature, the onset temperature of detectable SFD as $T_{C,\mathrm{SFD}}$. For example, $T_{C,\mathrm{SFD}} = 3.3 \pm 0.05$ K for sample No. 1, which is almost the same value as the bulk indium case, 3.4 K. This defined $T_{C,\mathrm{SFD}}$ is consistent with the onset temperature of vortex proliferation, which can be seen in the corresponding $\sigma_1(T)$ behavior and is shown later to be consistent with the STS measured transition temperature.

Sample No. 2 shows similarly low hole density, albeit with a slightly higher island density, compared with sample No. 1. The SFD result shows a comparable value, although $T_{C,\mathrm{SFD}}$ occurs at a slightly lower temperature, 2.95 ± 0.05 K, suggesting that an increase of scattering due to the increased island defects can suppress the T_C slightly but without impacting the SFD. From the two-fluid model fitting, the fitted zero-temperature SFD is 4.2 $\mu\mathrm{m}^{-2}$ [41], further testifying that this system is in the strong phase fluctuation limit. Interestingly, the dissipation component, $\sigma_1(T)$ in sample No. 1 shows a broader width than that in sample No. 2 despite having a slightly higher T_C; this might be related to a slightly larger width of grooves at the step edges in sample No. 1 which increases the phase fluctuations [42]. A dramatic change occurs in sample No. 3 when the hole density reaches 5%. Even though 95% of the surface retains its pristine single crystallinity, as shown by the atomic image, the SFD drops by almost 1 order of magnitude, signaling an enhancement of phase fluctuations. However, the onset SFD temperature $T_{C,\mathrm{SFD}}$, is reduced only by 2% and 12%, compared with samples No. 2 and No. 1, respectively. This shows that the local hole defects disturb the phase coherence and thus strongly suppress the global phase rigidity but has little effect on $T_{C,\mathrm{SFD}}$. More interestingly, upon a further increase of hole density to 6% [Fig. 2(d)], we found that the geometric arrangement of defects changes from a uniform distribution to defect chains forming closed loops, which break the continuous film into isolated patches. Although the crystallinity of the atomic structure is still preserved in the flat areas, we can no longer detect SFD down to the lowest instrumentation temperature. This systematic study indicates that both defect density and connectivity profoundly impact the phase rigidity in atomic layer superconductors—a point to be elaborated further below.

We next discuss the local superconducting gap. STS was used to probe the temperature dependent superconducting gap, $\Delta(T)$, using both a normal tip and a superconducting tip; the latter provides higher energy resolution with better accuracy of gap value determination (See Fig. S3 in Ref. [32]). Here, we present detailed results for sample No. 2 [Figs. 2(b) and 3(a)] and sample No. 3 [Figs. 2(c) and 3(b)], where the transition from high to low superfluid phase rigidity occurs. Figures 3(c) and 3(d) show the spectra acquired on sample No. 2 and No. 3 using a niobium (Nb) tip and a lead (Pb)-coated tungsten (W) tip, respectively, which exhibit SC-SC tunneling features [8], with four peaks at $\pm|\Delta_1 + \Delta_2|$ and $\pm|\Delta_1 - \Delta_2|$, where Δ_1 and Δ_2 refer to the superconducting gaps for tip and sample. A more accurate determination of Δ_2 is based on fitting a SC-SC tunneling formula, and the Fig. 3(e) inset shows one example (see Supplemental Material [32], Fig. S3b for detailed analysis). The Bardeen–Cooper–Schrieffer (BCS) fitting of the temperature dependent gap value $\Delta(T)$ [Figs. 3(e) and 3(f)] allows us to obtain the transition temperature for sample No. 2, $T_{C,\mathrm{BCS\_sample\,No.2}} = 3.1 \pm 0.1$ K, and for sample No. 3, $T_{C,\mathrm{BCS\_sample\,No.3}} = 2.9 \pm 0.2$ K [43].

Figure 3(g) summarizes the experimental determination of microscopic $T_{C,\mathrm{BCS}}$ (defined by the detectable energy gap) and macroscopic $T_{C,\mathrm{SFD}}$ (defined by the detectable SFD) as well as the SFD at 2.3 K for samples of different hole densities. Within the experimental error, we find that the values of $T_{C,\mathrm{BCS}}$ are consistent with the values of $T_{C,\mathrm{SFD}}$. In addition, in sample No. 4 where an SFD is not detectable down to 2.3 K, the SC gap is not observed down to 2.3 K either (see Supplemental Material [32], Fig. S4). These results indicate that a macroscopic detectable SFD goes hand in hand with a microscopic detectable SC gap. This observation is consistent with that in a 3D conventional superconductor [44], but directly contrasts with highly disordered 2D SC films, where the SC order parameter is spatially nonuniform [14,45]. We think the difference is related to the single-crystal nature of this system, where most of the film is well crystallized and connected, which leads to a uniform pairing potential and a coherent SC transition across the sample. In addition, the significant impact of hole defect density on the SFD is shown in Fig. 3(h).

We next discuss whether defects result in an inhomogeneity in the local tunneling gap. Figures 4(b) and 4(d) present the STS mappings across several atomic steps on sample No. 2 and several defects on sample No. 3, respectively. Since Δ_1 is the tip SC gap, the spatial uniformity of the sample SC gap Δ_2, is reflected in the uniformity of $\pm|\Delta_1 + \Delta_2|$ peak energies. As sample No. 2

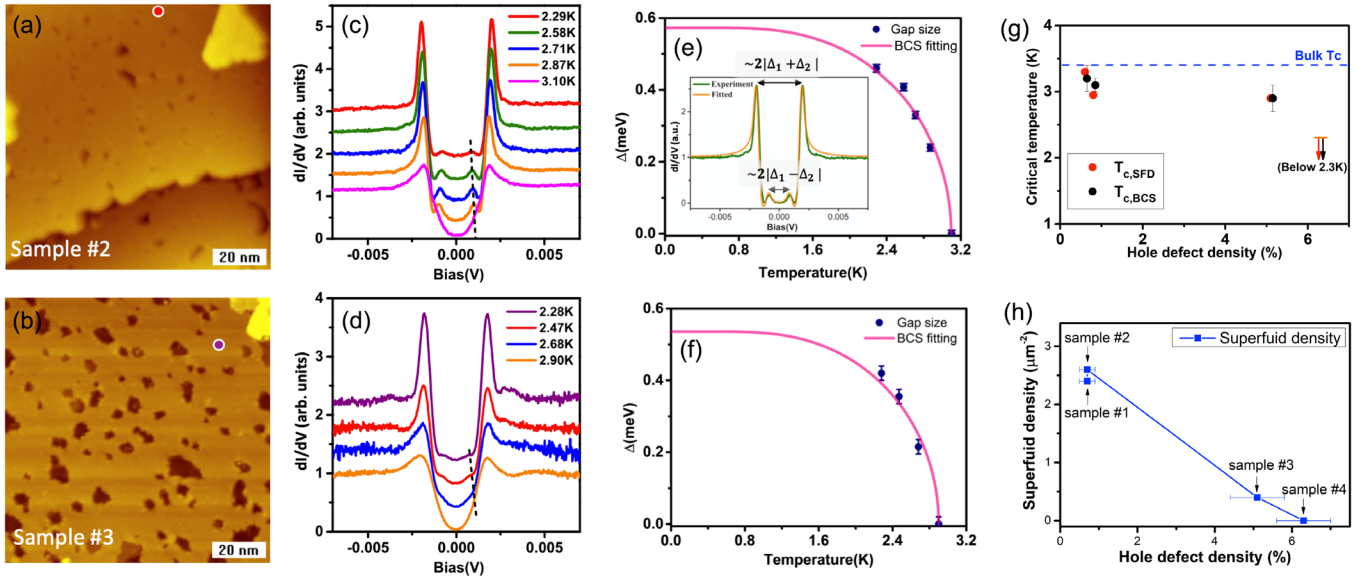

FIG. 3. Temperature dependent quasiparticle excitation spectrum. (a),(b) STM image taken on sample No. 2 and No. 3. (c),(d) Temperature dependent tunneling spectra on the pristine area of sample No. 2 and No. 3 using superconducting Nb and Pb tips, respectively. Spectra acquisition positions for 2.3 K are marked on (a) and (b) with the corresponding color. Spectra at other temperatures are also taken at a similar area, more than 10 nm away from the hole defects. Curves are offset for clarity. The black dashed line is a guide to show the temperature dependent $|\Delta_1 - \Delta_2|$ tunneling peak position. (e),(f) BCS gap fitting for sample No. 2 and No. 3, respectively. The inset in (e) shows a typical fitted result of a tunneling spectrum using superconducting Nb tip at 2.58 K. (g) A summary of critical temperatures $T_{C,SFD}$ and $T_{C,BCS}$ as a function of hole defect density. Data points for sample No. 1 and No. 2 are laterally offset to avoid overlapping, both are at 0.7% hole defect concentrations. (h) A summary of SFD at 2.3 K for samples of different hole defect density. Horizontal error bars represent statistical standard deviations of hole defect density.

contains primarily pristine regions, it might not be surprising that the gap uniformity is maintained even across the step edges [42,46]. Most surprisingly, this gap uniformity is maintained on sample No. 3, which contains 5% hole defects. Outside the gap energy range, the tunneling spectra exhibit a higher noise level at the defect locations. This is further exemplified by the STS spectra [Fig. 4(f)] acquired at a lower temperature and at three different representative positions [marked on Fig. 4(e)]: the pristine area, the step edge defect, and the hole defect. All three spectra show the typical superconductor to superconductor tunneling features with the same $\pm|\Delta_1 + \Delta_2|$ peak energies, indicating uniform gap values among these three points. Nevertheless, features near $\pm|\Delta_1 - \Delta_2|$ in the defect regions appear to be more smeared out, suggesting a weakening of order parameter coherence in the defect region without changing the gap size. As for the increased noise level outside the gap energy range, we attribute it to the enhanced local potential fluctuations due to the charging and de-charging process during tunneling [47]. Note that the uniformity of the SC gap is also maintained at 2.9 K, where we observed a vanishing of SC behavior both locally and globally. The reason why the same gap value is measured in the defect region may be closely related to a much longer coherence length, ~600 nm for a crystalline film [25,48], which is about 2 orders of magnitude larger than the defect size. This prevents local defects from disrupting the SC order parameter, although the defects can contribute to the reduction of SFD and the enhancement of phase fluctuations. On the other hand, the SC proximity effect from the surrounding continuous film may also play a role in retaining the SC gap value at the hole defects especially with the circular geometry of the hole defects, which is known to enhance the proximity effect due to an enhanced Andreev reflection [49].

This joint microscopic-macroscopic investigation provides us with a new insight into the role of nanohole defects on atomically thin 2D superconductors. We show that provided single crystallinity can be maintained over an extended region with very few defects, the T_c can remain relatively high (close to the bulk value) both at microscopic and macroscopic length scales. Nanohole defects, when uniformly dispersed, can reduce the superfluid density accordingly but with minor change in the T_c value based on the observable SFD at the macroscopic scale and superconducting gap at the microscopic scale. Most intriguingly, when defects form chain structures that break the surfaces into 2D patches with a lateral dimension of 100–200 nm, the superconducting gap and SFD vanish together. We believe this is due to the difficulty in forming a superconducting coherent state in the local region even though pristine single crystallinity is maintained (although the SC state may exist at a much lower temperature). Our work illustrates the profound impacts of nanohole defects

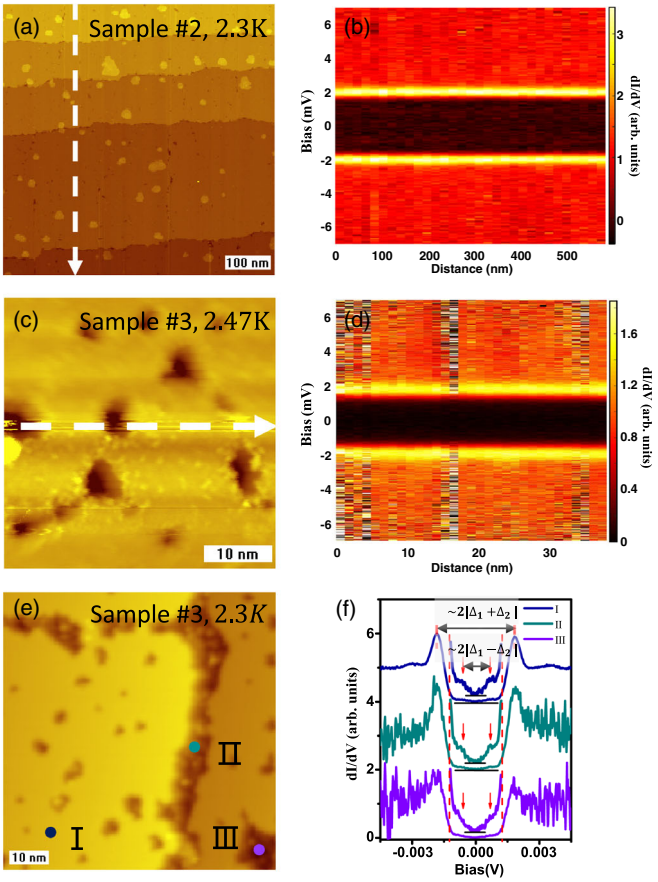

FIG. 4. Uniformity of superconducting gap distribution. (a),(c) STM image taken on sample No. 2 and No. 3. (b),(d) The spatial dependence of superconducting gap spectra along the white dashed arrow in (a) and (c), respectively. The position independent $\pm|\Delta_1 + \Delta_2|$ (bright yellow) peak energies show that the gap is spatially uniform. (e) Topography on sample No. 3 showing step edge defects and hole defects. (f) Spectra taken on position I to III as labeled in (e). Inside the window marked by the red dashed line, duplicate curves which are amplified by a factor of 7 are also plotted to better show the tunneling peak feature at $\pm|\Delta_1 - \Delta_2|$. Curves are offset for clarity and the horizontal black bars mark the zero for each curve.

on atomically thin 2D superconductors: both the density and the geometric arrangement of defects disrupt the formation of superconducting states. The overall picture presented here should be relevant to other types of condensates—such as exciton, magnon, and polariton condensates—in the extreme 2D limit.

We are grateful to Allan H. MacDonald, Ming Xie, and Takashi Uchihashi for helpful discussions. This work was primarily supported by the National Science Foundation through the Center for Dynamics and Control of Materials: an NSF MRSEC under Cooperative Agreement No. DMR-1720595. Other support was from NSF Grants No. DMR-1808751, No. DMR-1949701, No. DMR-2114825, and the Welch Foundation F-1672.

[1] P. W. Anderson, J. Phys. Chem. Solids **11**, 26 (1959).
[2] I. Hetel, T. R. Lemberger, and M. Randeria, Nat. Phys. **3**, 700 (2007).
[3] M. Mondal, A. Kamlapure, M. Chand, G. Saraswat, S. Kumar, J. Jesudasan, L. Benfatto, V. Tripathi, and P. Raychaudhuri, Phys. Rev. Lett. **106**, 047001 (2011).
[4] M. Sahoo and D. Behera, J. Supercond. Novel Magn. **27**, 83 (2014).
[5] Y. Fang, C. T. Wolowiec, D. Yazici, and M. B. Maple, Nov. Supercond. Mater. **1**, 79 (2015).
[6] D. Torsello, L. Gozzelino, R. Gerbaldo, T. Tamegai, and G. Ghigo, Sci. Rep. **11**, 5818 (2021).
[7] J. Simonin, Phys. Rev. B **33**, 7830 (1986).
[8] M. Tinkham, *Introduction to Superconductivity,* 2nd ed. (Dover, Mineola, New York, USA, 2015).
[9] V. J. Emery and S. A. Kivelson, Nature (London) **374**, 434 (1995).
[10] A. E. White, R. C. Dynes, and J. P. Garno, Phys. Rev. B **33**, 3549 (1986).
[11] D. B. Haviland, Y. Liu, and A. M. Goldman, Phys. Rev. Lett. **62**, 2180 (1989).
[12] S. J. Turneaure, T. R. Lemberger, and J. M. Graybeal, Phys. Rev. Lett. **84**, 987 (2000).
[13] R. W. Crane, N. P. Armitage, A. Johansson, G. Sambandamurthy, D. Shahar, and G. Grüner, Phys. Rev. B **75**, 094506 (2007).
[14] B. Sacépé, C. Chapelier, T. I. Baturina, V. M. Vinokur, M. R. Baklanov, and M. Sanquer, Phys. Rev. Lett. **101**, 157006 (2008).
[15] J. Yong, T. R. Lemberger, L. Benfatto, K. Ilin, and M. Siegel, Phys. Rev. B **87**, 184505 (2013).
[16] J. M. Graybeal and M. R. Beasley, Phys. Rev. B **29**, 4167 (1984).
[17] A. Frydman, Physica (Amsterdam) **391C**, 189 (2003).
[18] H. Nam *et al.*, Proc. Natl. Acad. Sci. U.S.A. **113**, 10513 (2016).
[19] S. Qin, J. Kim, Q. Niu, and C.-K. Shih, Science **324**, 1314 (2009).
[20] T. Zhang *et al.*, Nat. Phys. **6**, 104 (2010).
[21] H. Nam, H. Chen, P. W. Adams, S.-Y. Guan, T.-M. Chuang, C.-S. Chang, A. H. MacDonald, and C.-K. Shih, Nat. Commun. **9**, 5431 (2018).
[22] Q. Y. Wang *et al.*, Chin. Phys. Lett. **29**, 037402 (2012).
[23] M. Liao *et al.*, Nat. Phys. **14**, 344 (2018).
[24] T. Uchihashi, P. Mishra, M. Aono, and T. Nakayama, Phys. Rev. Lett. **107**, 207001 (2011).
[25] M. Yamada, T. Hirahara, and S. Hasegawa, Phys. Rev. Lett. **110**, 237001 (2013).
[26] Y. Wu *et al.*, Phys. Rev. B **99**, 140506 (2019).
[27] J. W. Park and M. H. Kang, Phys. Rev. Lett. **109**, 166102 (2012).
[28] T. Uchihashi, P. Mishra, and T. Nakayama, Nanoscale Res. Lett. **8**, 167 (2013).
[29] A. F. Hebard and A. T. Fiory, Phys. Rev. Lett. **44**, 620(E) (1980).
[30] B. Jeanneret, J. L. Gavilano, G. A. Racine, C. Leemann, and P. Martinoli, Appl. Phys. Lett. **55**, 2336 (1989).
[31] H. Nam, P.-H. Su, and C.-K. Shih, Rev. Sci. Instrum. **89**, 043901 (2018).
[32] See Supplemental Material at http://link.aps.org/supplemental/10.1103/PhysRevLett.127.127003 for

additional information on materials, instrumentations, and data analysis.
[33] S. J. Turneaure, E. R. Ulm, and T. R. Lemberger, J. Appl. Phys. **79**, 4221 (1996).
[34] G. Logvenov, A. Gozar, and I. Bozovic, Science **326**, 699 (2009).
[35] J.-F. Ge, Z.-L. Liu, C. Liu, C.-L. Gao, D. Qian, Q.-K. Xue, Y. Liu, and J.-F. Jia, Nat. Mater. **14**, 285 (2015).
[36] J. M. Kosterlitz and D. J. Thouless, J. Phys. C **6**, 1181 (1973).
[37] J. Pearl, Appl. Phys. Lett. **5**, 65 (1964).
[38] D. R. Nelson and J. M. Kosterlitz, Phys. Rev. Lett. **39**, 1201 (1977).
[39] B. I. Halperin and D. R. Nelson, J. Low Temp. Phys. **36**, 599 (1979).
[40] L. Benfatto, C. Castellani, and T. Giamarchi, Phys. Rev. Lett. **98**, 117008 (2007).
[41] The slightly higher value compared to sample No. 1 may come from a less accurate fitting due to the limited experimental temperature range.
[42] S. Yoshizawa, H. Kim, T. Kawakami, Y. Nagai, T. Nakayama, X. Hu, Y. Hasegawa, and T. Uchihashi, Phys. Rev. Lett. **113**, 247004 (2014).
[43] The enlarged error bar here is due to a less accurate fitting originating from the weaker superconductor to the superconductor tunneling feature.
[44] J. Bardeen, L. N. Cooper, and J. R. Schrieffer, Phys. Rev. **108**, 1175 (1957).
[45] V. F. Gantmakher and V. T. Dolgopolov, Phys. Usp. **53**, 1 (2010).
[46] C. Brun *et al.*, Nat. Phys. **10**, 444 (2014).
[47] F. Massee, Y. K. Huang, M. S. Golden, and M. Aprili, Nat. Commun. **10**, 544 (2019).
[48] E. Rotenberg, H. Koh, K. Rossnagel, H. W. Yeom, J. Schafer, B. Krenzer, M. P. Rocha, and S. D. Kevan, Phys. Rev. Lett. **91**, 246404 (2003).
[49] J. Kim, V. Chua, G. A. Fiete, H. Nam, A. H. MacDonald, and C.-K. Shih, Nat. Phys. **8**, 464 (2012).